ELSEVIER

Contents lists available at ScienceDirect

# Sensing and Bio-Sensing Research

journal homepage: www.elsevier.com/locate/sbsr





# Application of novel oligomeric Co(II) complexes of 4,4'-bipyridine and 1,10-phenanthroline modified glassy carbon electrode for differential pulse voltammetric determination of ciprofloxacin

Mezgebu Biresaw<sup>a</sup>, Adane Kassa<sup>b,\*</sup>, Getinet Tamiru Tigineh<sup>a</sup>, Atakilt Abebe<sup>a,\*</sup>

- <sup>a</sup> Chemistry Department, College of Sciences, Bahir Dar University, Bahir Dar, Ethiopia
- b Department of Chemistry, College of Natural and Computational Sciences, Debre Markos University, P.O. Box 269, Debre Markos, Ethiopia

#### ARTICLE INFO

#### Keywords: Electrochemical determination Ciprofloxacin Poly(µ-4,4'-bipyridine(bis(1,10phenanthroline))cobalt(II)chloride)) Glassy carbon electrode Tablet formulations

#### ABSTRACT

Two new oligomer mixed ligand complexes, comprising 21 ([Co<sub>21</sub>(phen)<sub>42</sub>(bipy)<sub>21</sub>]Cl<sub>42</sub> (C2)) and 100 monomer units ( $[Co_{100}(phen)_{200}(bipy)_{100}]Cl_{200}$  (C3)) were synthesized. These complexes, designated as  $[Co_{21}(phen)_{42}(-bipy)_{4$ bipy)21]Cl42 (C2) and [Co100(phen)200(bipy)100]Cl200 (C3), were employed for the modification of a glassy carbon electrode (GCE) to detect ciprofloxacin (CPF) in tablet formulations and human urine samples. By potentiodynamic deposition, the modified electrodes (poly(C2)/GCE) and (poly(C3)/GCE) were prepared, forming a conductive electroactive film on the GCE surface. The modified electrodes were characterized using cyclic voltammetry and electrochemical impedance spectroscopy, which revealed an increased effective surface area and a significant reduction in charge transfer resistance of the electrode. An oxidative peak at a lower potential with a six-fold increase in peak current was observed at the poly(C2)/GCE. The absence of a reductive peak in the reverse scan indicated the irreversibility of the electrochemical oxidation of CPF. The correlation coefficient between the peak current and the square root of the scan rate indicated that CPF oxidation at the poly (C2)/GCE was primarily controlled by diffusion mass transport. With a detection limit of 3.4  $\times$  10<sup>-9</sup> M, the voltammetric current response of CPF at the poly(C2)/GCE under optimal circumstances showed a linear trend with concentrations ranging from  $5.0 \times 10^{-8}$  to  $2.0 \times 10^{-4}$  M. It was discovered that the CPF levels in the examined tablet brands fell between 98.35 % and 101.30 % of their stated ranges. The recovery results for tablet and urine samples ranged from 99.44 % to 99.95 % and 99.25 % to 100.51 %, respectively, with interference recovery showing an error of less than 4.73 %. When it came to determining CPF in tablet formulations and human urine samples, the new approach outperformed recently published voltammetric methods. This superiority can be attributed to the simplicity of the electrode modification step, the lowest limit of detection, and a reasonably wide linear dynamic range.

# 1. Introduction

Both natural and synthetic polynuclear transition metal complexes possess appealing characteristics such as a significantly available surface area [13], excellent chemical stability [21], and favorable electro- and photo-catalytic activity [29,37]. These features have enabled their application in various fields. For example, polynuclear transition metal complexes are found in numerous enzymes that serve as functional centers and contribute to structural stability [42]. Based on these observations, biomimetic catalysis has been explored via the synthesis of polynuclear transition metal complexes over the past few decades [34]. These complexes exhibit cooperative interactions between the monomer

units, resulting in materials with enhanced polymer characteristics [7]. In this respect, the coordination chemistry of mixed ligand complexes has attracted the attention of many investigators due to the acquisition of desired properties. Mixed ligand metal complexes are compounds that consist of more than one type of ligand coordinated to the same metal ion exhibiting unique features with a distinct set of characteristics resulting from the complementary combination of the different properties of the ligands and the metal ion. As a result, the complexes often display improved properties, such as electrochemical activities as valuable electrode modifiers, compared to homoleptic complexes. By employing metal complex-modified electrodes, the effective surface area and catalytic properties can be augmented. This enhancement leads to a

E-mail addresses: adane\_kassa@dmu.edu.et (A. Kassa), atakiltabebe1@gmail.com (A. Abebe).

<sup>\*</sup> Corresponding authors.

significant improvement in electrode activity, enhancing selectivity, stability, sensitivity, and reproducibility. Achieving these enhancements involves a meticulous selection of the transition metal and ligands to create a product with polymerizable electroactivity and a geometry that fosters a porous and expansive surface area on the electrode. This configuration facilitates heightened charge movement throughout the polymer, featuring appropriate redox potentials to facilitate the oxidation or reduction of analytes present in the tested samples. For these purposes, mixed ligand oligomeric complexes were prepared by identifying cobalt(II), 4,4'-bipyridine, and 1,10-phenanthroline as proper precursor materials.

The compound 1,10-phenanthroline (phen) is a moderately rigid tricyclic heteroaromatic molecule. It possesses strategically positioned nitrogen atoms with lone pairs of electrons, making it electron-deficient and displaying  $\pi$ -acidic properties [1]. This electron-deficient nature allows it to readily accept electrons from coordinated metals, influencing the electrochemistry of the resulting compound. 4,4′-bipyridine (4,4′-bipy) (as shown in scheme SM1A) is a flexible heterocyclic compound derived from two pyridine molecules connected by a C—C bond. It contains nitrogen atoms with lone pairs of electrons, making it a suitable bridging ligand for network formation. The rotational freedom of its pyridine moieties along the C—C bond facilitates the formation of twisted conformations in bridged monomer complexes, which are conducive to charge movement throughout the complex [2].

Ciprofloxacin (as shown in scheme SM1B) belongs to the fluoroquinolones class of drugs and exhibits broad-spectrum antibacterial activity against Gram-negative and Gram-positive bacteria. It functions by inhibiting bacterial growth and is used for the treatment of infections in humans and animals. CPF demonstrates relatively low resistance compared to several other antibiotics, including penicillin, cephalosporin, and aminoglycosides. Common side effects of CPF include nausea, diarrhea, dizziness, lightheadedness, headache, and trouble sleeping. Due to the substantial excretion of unchanged ciprofloxacin (CPF), environmental contamination is a significant concern. Additionally, the liver metabolizes CPF into at least four partially modified forms by altering the piperazinyl group. These metabolites, including *N*-acetyl ciprofloxacin, Oxo-ciprofloxacin, desethylene ciprofloxacin, and sulfociprofloxacin, are also excreted, further contributing to environmental pollution. This issue is exacerbated by improper CPF usage practices, such as its unauthorized consumption without a prescription, improper dosing, and the utilization of leftover medication.[15,17].

Consequently, monitoring CPF levels in pharmaceutical formulations, biological samples, and other matrices has garnered research interest. Various methods such as liquid chromatography [17,36], capillary electrophoresis [27,28], and spectrophotometry [16,32] have been employed for CPF detection in different samples. However, these methods are not environmentally friendly because they frequently need the use of substantial volumes of organic solvents. Additionally, they can be cost-ineffective due to the requirement of expensive instruments and long analysis times. In this context, electrochemical techniques are preferable due to their accuracy, reproducibility, sensitivity, stability, selectivity, environmentally friendly nature, and low instrumental costs [9,24,33].

Numerous researchers have explored the detection of ciprofloxacin using electrochemical sensing techniques. Chauhan and colleagues demonstrated CPF detection through a reduced graphene oxide/poly (phenol red) modified glassy carbon electrode [10]. Xie et al. showcased electrochemical detection of ciprofloxacin using a graphene-modified glassy carbon electrode [41]. Chuiprasert et al. developed an electrochemical sensor for CPF detection using a copper-iron mixed metal oxide nanoparticles/reduced graphene oxide composite [11]. Khaleque et al. reported CPF sensing with an MXene (Ti<sub>3</sub>C<sub>2</sub>Tx)/poly (rutin) composite as an electrode material [25]. Furthermore, Gissawong and team presented an electrochemical sensor for voltammetric detection of ciprofloxacin using a glassy carbon electrode modified with activated carbon, gold nanoparticles, and a supramolecular solvent [19]. These

studies highlighted the potential of electrochemical methods for CPF detection. However, the electrode preparation procedures in these studies were either costly or time-consuming. Therefore, there is a need for a more efficient method that addresses these limitations. Consequently, a method with low equipment costs, quick preparation time, and environmentally friendly characteristics was pursued and is discussed here. In this study, two oligomeric polynuclear complexes were synthesized from a previously reported monomer complex with the formula [Co(phen)2(H2O)2)]Cl2(C1), which was prepared through the coordination of phen to Co(II) using a high dilution method [5]. Refluxing this monomer complex with 4,4'-bipyridine resulted in the formation of oligomeric complexes, which were examined for their capacity to be used in altering electrode surfaces for the straightforward and selective measurement of CPF in human urine samples and four different brands of tablets. The experimental conditions, including solution parameters, were optimized for this purpose.

The synthesized complex,  $[Co_{21}(phen)_{42}(bipy)_{21}]Cl_{42}$  (C2) was subjected to potentiodynamic electropolymerization on a glassy carbon electrode, resulting in the formation of an electroactive film surface, which significantly improved the sensitivity of the electrode. This improvement was observed through noticeable changes in the overpotential reduction and the increased peak current during the electrochemical analysis. Moreover, this work presented a method with the lowest detection limit (LoD) and with the lowest starting concentration of the dynamic range compared to all the previous works.

# 2. Materials and methods

#### 2.1. Apparatus and chemicals

All chemicals and reagents utilized in this study were of analytical grade and were employed without any additional purification. The following substances were used: Ciprofloxacin (≥99.0 % purity, Sigma Aldrich), CoCl<sub>2</sub>.6H<sub>2</sub>O (98 % purity, ACS reagent), 1,10-phenanthroline monohydrate (≥99.7 % purity, Sigma Aldrich), methanol (100 % purity, Loba Chemicals (p) Ltd), 4,4'-bipyridine (>99 % purity, Fisher Scientific), acetonitrile (Sigma Aldrich), dimethyl formamide (DMF) (>99 % purity, Loba Chemicals (p) Ltd), dimethyl sulfoxide (DMSO) (95 % purity, Loba Chemicals (p) Ltd), dichloromethane (>99 % purity), chloroform, HClO<sub>4</sub> (70 % purity), potassium chloride (99.5 % purity, Blulux Laboratories (p) Ltd), sodium monohydrogen phosphate, and sodium dihydrogen phosphate (>98.0 % purity, Blulux Laboratories (p) Ltd), hydrochloric acid (37 % purity, Fisher Scientific), sodium hydroxide (Extra pure, Lab Tech Chemicals), nitric acid (70 % purity, Fisher Scientific), K<sub>3</sub>[Fe(CN)<sub>6</sub>] and K<sub>4</sub>[Fe(CN)<sub>6</sub>] (98.0 % purity, BDH Laboratory Samples, England), ethanol (CARLOERBA Reagents S.A.S, France), AgNO<sub>3</sub> (≥99.0 % purity, Sigma Aldrich).

The following equipment and instruments were used: a centrifuge (1020D, Centurion Scientific LTD, UK), an ICP-OES spectrometer (PerkinElmer, Optima 7300V HF Version), CHI 760E potentiostat (Austin, Texas, USA), a portable pH/conductivity/TDS meter (Bante901P), an electronic balance (Nimbus, ADAM Equipment, USA), a deionizer (Evoqua Water Technologies), an FT-IR spectrophotometer (Cary 60, Agilent Technologies), an FT-IR spectrophotometer (PerkinElmer, BX), an ICP-OES spectrometer (PerkinElmer, AD 8000, Romania), an atomic absorption spectrometry (AAS) (PerkinElmer, AAnalyst 800), and a melting point apparatus (Stuart SMP30).

# 2.2. Electrochemical measurement

The electrochemical measurements were conducted using a three-electrode setup, consisting of a Pt coil as the counter electrode, Ag/AgCl (3.0 M KCl) as the reference electrode, and either a bare glassy carbon electrode (GCE) or a poly(C2)/GCE as the working electrode. The modified GCE was characterized using electrochemical impedance spectroscopy (EIS) and cyclic voltammetry (CV) techniques. In order to

quantify CPF in human urine samples and pharmaceutical tablet formulations, the differential pulse voltammetry (DPV) approach was utilized.

#### 2.3. Procedure

# 2.3.1. Metal complex synthesis

A modified version of  $[Co(phen)_2(H_2O)_2]Cl_2(C1)$  (cobalt(II) chloride complex with diaquabis(1,10-phenanthroline)), was prepared following a previously reported method [5], with some adjustments. In a 250 mL round bottom flask, a solution of 1,10-phenanthroline monohydrate (0.85 g, 2.14 mmol) in ethanol (30.0 mL) was added slowly using a dropping funnel to a magnetically stirred solution of  $CoCl_2.6H_2O$  (0.51 g, 2.14 mmol) in 30 mL ethanol. The stirring was continued for 12 h at room temperature, resulting in the formation of a reddish-brown homogeneous solution. The solvent was then removed using a rotary evaporator under vacuum, yielding a dark red powder (yield: 1.01 g).

Next, a solution of 4,4'-bipy (0.42 g, 1.33 mmol) in ethanol (50.0 mL) using a dropping funnel was added to a solution of C1 (0.75 g, 1.33 mmol) in 50 mL ethanol in a 250 mL round bottom flask, while stirring. The stirring was continued for 24 h at room temperature, resulting in the formation of a light red homogeneous solution. The solution was then refluxed in an oil bath at 80  $^{\circ}$ C for 8 h. Afterward, the reaction solution was allowed to stand overnight to cool to room temperature. This process yielded a white precipitate and a reddish-brown solution. The precipitate was separated by filtration using a Whatman filter paper, resulting in the formation of a pinkish white powder (C3) (yield: 0.18 g). The solvent in the reddish-brown filtrate was removed using a rotary evaporator, collecting a light red solid powder (C2) (yield: 0.82 g). The path of the synthesis of the complexes is indicated in Fig. 1.

#### 2.3.2. Complex characterization procedures

To estimate the ionizable chloride content, a 10 mg sample of the complex was dissolved in 30 mL distilled water. Excess AgNO $_3$  solution was added, resulting in the formation of a precipitate called silver halide (AgCl). The crude precipitate was filtered and then dried in an oven at 110  $^{\circ}$ C. The amount of chloride present was determined gravimetrically.

The Adwa AD 8000 pH/mv/EC/TDS meter was used to measure the electrolytic conductance of each complex in a 0.1 mM solution in

deionized water at room temperature. A 1.0 mM solution of each species (salt, ligands, and produced complexes) in ethanol was used to record UV–Vis electronic spectra. With the use of a Cary 60 UV–Vis spectro-photometer, measurements were made in the 200–800 nm range. About 0.001 g of each sample was combined with 0.2 g of KBr to create discs, and the IR spectra were taken. The measurements were made between 400 and 4000  ${\rm cm}^{-1}$  using a BX spectrophotometer.

 $0.01~{\rm g}$  of each complex was combined with 5.0 mL of concentrated nitric acid in order to estimate the cobalt level in every one complex via atomic absorption spectrometry (AAS). Gently heating the mixture in a 50 mL conical flask until very few drops were left. The nitric acid digestion procedure was carried out three times in order to eliminate every organic component present in the complex. In a 50 mL volumetric flask, the leftover residue was reconstituted and diluted with deionized water to the appropriate level. A Stuart SMP30 melting point apparatus was used to find the compounds' melting points.

# 2.3.3. Preparation of poly(C2)/GCE

A highly polished glassy carbon electrode with a mirror-like finish was placed in a 0.1 M phosphate buffer (PB) with a pH of 7.0. The solution contained 1.0 mM of C2. The electrode was then subjected to 15 cycles of scanning within an optimized potential range of -1.2 V to +1.8 V at a scan rate of 100 mV s $^{-1}$ . Following this, the poly(C2)/GCE was washed with deionized water and allowed to stabilize in 0.5 M  $\rm H_2SO_4$  between -0.80 V and +0.80 V potential range until a stable CV was produced. After that, the modified electrode was allowed to dry properly and made ready for more tests. To make GCE modified with poly(phen), poly(4,4'-bpy), poly(C1), electrodeposited Co(0), and poly (C3), the same approach was repeated. A 1.0 mM solution of the corresponding monomer in pH 7.0 PB was used in each instance.

# 2.3.4. Standard CPF solution preparation

The preparation of a stock solution involved dissolving 165.67 mg of CPF in 100 mL of deionized water, resulting in a concentration of 5.0 mM for the standard. Working standard solutions were then prepared by performing serial dilutions using PB at the desired pH levels, starting from the stock solution.

Fig. 1. The synthesis path of the complexes

#### 2.3.5. Preparation of real samples

Four brands of CPF tablets, namely Bruce (from an Indian pharmaceutical factory), Ciplet (from Sansheng Pharmaceutical Plc, China), Aarciflox (Germany), and Zindolin (Remedica Ltd., Cyprus), were purchased from a local drug store in Bahir Dar city, Ethiopia. That were labeled as 500 mg CPF/tablet and had average tablet masses of 577.6 mg (Bruce), 610.8 mg (Ciplet), 591.5 mg (Aarciflox), and 583.7 mg (Zindolin). Using a mortar and pestle, the pills were crushed and made uniform.

For each brand, a stock solution of CPF tablet samples with a concentration of 2.0 mM was prepared. This was achieved by transferring an accurately weighed tablet powder equivalent to 66.27 mg (76.56 mg for Bruce, 80.96 mg for Ciplet, 78.40 mg for Aarciflox, and 77.36 mg for Zindolin) of CPF to a 100 mL volumetric flask and filling it with deionized water. Serial dilution was then used to create working tablet sample solutions at pH 7.0 in PB from the corresponding stock solutions.

An adult volunteer provided a fresh sample of human urine, which was centrifuged for ten minutes at 4000 rpm. A 25 mL volumetric flask was filled with 0.5 mL of the supernatant, which was then diluted with pH 7.0 PB. For spike recovery analysis, urine samples spiked with standard CPF at various concentrations (0.0, 20.0, 40.0, and 80.0  $\mu M)$  were produced.

# 3. Results and discussion

# 3.1. C2 synthesis

### 3.1.1. Synthesis mechanism

As illustrated in Eqs. (1) and (2) (Fig. 1), the new C2 complex was synthesized via a two-step process employing phen, 4,4'-bipy, and CoCl<sub>2</sub>.6H<sub>2</sub>O as raw ingredients. Table SM1 provides an overview of the produced complexes' physico-chemical characteristics.

$$CoCl2.6H2O + 2phen.H2O \rightarrow [Co(phen)2(H2O)2]Cl2(C1)$$
 (1)

$$\begin{split} 121\text{C1} + 121(4,4'-bipy) &\rightarrow \left[\text{Co}_{21}(\text{phen})_{42}(\text{bipy})_{21}\right] \text{Cl}_{42} \text{ (C2)} \\ &+ \left[\text{Co}_{100}(\text{phen})_{200}(\text{bipy})_{100}\right] \text{Cl}_{200} \text{ (C3)} \end{split} \tag{2}$$

(Note: The subscripts in the above equations indicate the number of metal ions, each ligand, and the counter anion present in each complex)

The complexes exhibited different colors and decomposition (melting) points, indicating their distinct characteristics (Table SM1). They were soluble in water, ethanol, methanol, and DMSO, while insoluble in chloroform, acetone, acetonitrile, dichloromethane, and dimethylformamide (DMF). This suggests the polar nature of the complexes. The formation of white precipitate upon treating each complex with an excess aqueous solution of AgNO<sub>3</sub> confirmed the presence of chloride ions outside the coordination sphere of the complexes. The determination of chloride content through gravimetric analysis, along with the results from the electrolytic conductivity experiment, aided in quantifying the amount of chloride in the outer sphere of the complexes (Table SM1).

These findings were further supported by the metal estimation experiment using AAS. The conductivity values discovered during the study of electrolytic behavior demonstrated the complexes' capacity to ionize. Notably, the conductivity of C2 was 5.6 times higher than that of C1, suggesting a significant increase in the release of ions during dissolution. However, C3 showed lower conductivity than C1, perhaps because of the bigger cation's decreased mobility in the solution, even though it contained a larger amount of Co(II) (see Tables SM2 and SM1).

In the AAS determination of cobalt content, samples of C1, C2, and C3 weighing  $0.02\,\mathrm{mg}$ ,  $0.002\,\mathrm{mg}$ , and  $0.001\,\mathrm{mg}$ , respectively, were used. Interestingly, even though the mass of C2 was one-tenth of C1, the absorbance by the metal ion increased from  $1.030\,\mathrm{ppm}$  to  $2.173\,\mathrm{ppm}$ , nearly doubling it. This indicates a twentyfold higher cobalt concentration in the second complex compared to the first complex (refer to

Table SM2). Similarly, despite the mass of C3 being one-twentieth of C1, the recorded metal ion concentration was 5.150 ppm, indicating a nearly fivefold higher cobalt concentration compared to C1. This confirms the presence of 100 monomer units in C3 (refer to Table SM2). The combination of these findings with the halide estimation experiment suggests that the formulas for C2 and C3 are  $[Co_{21}(phen)_{42}(bipy)_{21}]Cl_{42}$ , and  $[Co_{100}(phen)_{200}(bipy)_{100}]Cl_{200}$ , respectively.

# 3.1.2. Characterization of synthesized complex

3.1.2.1.~UV-Vis. Changes in the complexes, ligands, and salt electronic spectra, such as shifts and alterations in characteristic resonance absorption bands, can provide insights into the electronic environment of the reactants. These changes are helpful in determining the happening of the reaction and elucidating the structure. In the UV–Vis spectrum, the bands observed at 228 nm and 264 nm in the phen spectrum, corresponding to  $\pi \to \pi^*$  and  $n \to \pi^*$  transitions, respectively (see Fig. SM1A), alongside to the bands observed at 428 nm, 539 nm, and 577 nm in the salt spectrum due to d-d transitions, were no longer present (see Fig. SM1B) [4,18,38].

Additionally, the bands observed at 240 nm and 330 nm, which match to ligand ( $H_2O$ ) to metal (Co(II)) charge transfer, experienced a shift to 306 nm and 346 nm, respectively, indicating a metal to ligand (phen) transition (see Fig. SM1C). This shift suggests the coordination of phen to Co(II) to form the complex [ $Co(phen)_2(H_2O)_2$ ]Cl<sub>2</sub>.

The band observed at 306 nm (MLCT) in the spectrum of C1 underwent a blue shift to 301 nm (MCLT) after treatment with 4,4′-bipy (Fig. SM1D). In the spectrum of 4,4′-bipy, the band observed at 290 nm corresponding to  $\pi\to\pi^*$  either disappeared or shifted and became obscured in the 301 nm (MLCT) band of C3 (Fig. SM1E). Interestingly, the band that appeared at 301 nm in the spectrum of C3 experienced a further blue shift to 287 nm in the spectrum of C2 (Fig. SM1F). This shift can be attributed to the coordination of a greater number of 4,4′-bipy molecules, which causes the blue shift to occur.

3.1.2.2. FT-IR. Infrared spectroscopy is employed to determine whether complexation has occurred by examining shifts in vibrational frequencies, changes in the strength of characteristic bands of the ligand, and the emergence or elimination of bands specific to precursor molecules. The bands at 1637 cm $^{-1}$  (s) and 1587 cm $^{-1}$  (s), characteristic of  $\nu\text{C=C}$  in free phen (Fig. SM2A), exhibit changes in intensity and wave number to 1636 cm $^{-1}$  (w) and 1587 cm $^{-1}$  (w), respectively, in [Co (phen)2(H2O)2]Cl2 (Fig. SM2B) [5,12]. Additionally, the band at 3045 cm $^{-1}$  corresponding to  $\nu\text{C-H}$  in the free phen spectrum is observed to undergo a blue shift to 3052 cm $^{-1}$ . These blue shifts in  $\nu\text{C=C}$  and  $\nu\text{C-H}$  indicate an increase in bond order for C=C due to electron flow from the electron-rich metal center to the electron-deficient phen via  $\pi\text{-back}$  bonding.

The bands at 1510 cm<sup>-1</sup> (s) and 1346 cm<sup>-1</sup> in the spectrum of free phen, corresponding to  $\nu C{=}N$  and  $\nu C{-}N$  (Fig. SM2A), respectively, undergo shifts to 1505 cm<sup>-1</sup> (w) and 1341 cm<sup>-1</sup> (vw) in the spectrum of [Co(Phen)2(H2O)2]Cl2 (Fig. SM2B), indicating changes in their bond nature due to ligand coordination with the metal ion. The blue shift observed in  $\nu C=N$  suggests an increase in bond order caused by electron flow from the filled t2g orbitals to the ligand, while the red shift observed in vC-N is attributed to increased mass resulting from coordination of N to the metal ion. Furthermore, the decrease in intensity of the band at 1433 cm<sup>-1</sup> in the C1 spectrum can be attributed to a change in the dipole moment following ligand coordination with the metal ion. The band at 3433 cm $^{-1}$  corresponding to  $\nu$ O-H of the coordinated water in the free ligand, where water is linked to N of phen via hydrogen, experiences a red shift to 3370 cm<sup>-1</sup> in C1, where water is coordinated to the metal center via oxygen. The new band appearing at 409 cm<sup>-1</sup> represents vCo-N, as shown in Fig. SM2B.

Regarding the instance of 4,4'-bipy (Fig. SM2C), the bands at 1596

cm<sup>-1</sup> (s) and 1412 cm<sup>-1</sup> (s), characteristic of  $\nu$ C=C and  $\nu$ C=N, respectively, in the free molecule, exhibit shifts to 1596 cm<sup>-1</sup> (w) and 1401 cm<sup>-1</sup> (w), respectively, in [Co<sub>21</sub>(phen)<sub>42</sub>)(bipy)<sub>21</sub>]Cl<sub>42</sub> (Fig. SM2D), indicating coordination. Furthermore, the bands observed at 407 cm<sup>-1</sup>, 406 cm<sup>-1</sup>, and 508 cm<sup>-1</sup> certify the creation of Co—N bonds following reactions with the ligands [30]. The increase in wave numbers after coordination of 4,4′-bipy can be justified in a similar manner as with phen. With the exception of higher band intensities, which suggest a greater number of components causing the absorption, C3's spectrum resembles that of C2. For example, the intensities of bands corresponding to  $\nu$ C-H,  $\nu$ C=C, and  $\nu$ C=N show significant increases. Moreover, the broad bands around 3300–3450 cm<sup>-1</sup> in Fig. SM2C-E could be associated with  $\nu$ O-H of the adsorbed water on KBr.

According to the findings of the halide estimation experiment, the cation to anion ratios for C1, C2, and C3 were, in that order, 1:2, 1:42, and 1:200. Additionally, the degree of polymerization in C2 and C3, determined through AAS data, revealed that C2 is composed of twenty-one monomer units, while C3 is composed of one hundred monomer units. These pieces of evidence, along with data from FT-IR, UV–Vis, and electrolytic conductivity measurements, work together to confidently propose the formula of the complexes as  $[Co(phen)_2(H_2O)_2]Cl_2$ ,  $[Co_{21}(Phen)_{42}(bipy)_{21}]Cl_{42}$  and  $[Co_{100}(Phen)_{200}(bipy)_{100}]Cl_{200}$ . These evidences allow the structure of the complexes as shown in scheme SM2 to be proposed.

# 3.2. Fabrication of the poly(C2)/GCE

The film thickness is among the most key variables in potentiodynamically depositing a modifying material on the electrode surface. This is especially important when intending to deposit the GCE surface with poly(C2) film. Thus, the film thickness may be controlled by tracking the peak growth and enhancing the modified electrode's current response to CPF as a probe considering the quantity of scan cycles. The current response of poly(C2)/GCE for CPF at different polymerization scan cycles (10–25) is shown in Fig. SM3. The anodic peak current of CPF is increase with varying slope from 10 to 25 scan cycles (Inset of Fig. SM3A & B), making 15 scan cycles to be the most optimal in this experiment with potential and current advantages.

Repetitive CVs of GCE in pH 7.0 PBS containing 1.0 mM C2 are shown in Fig. 2 scanned between -1.2 and +1.8 V for 15 cycles. Curves

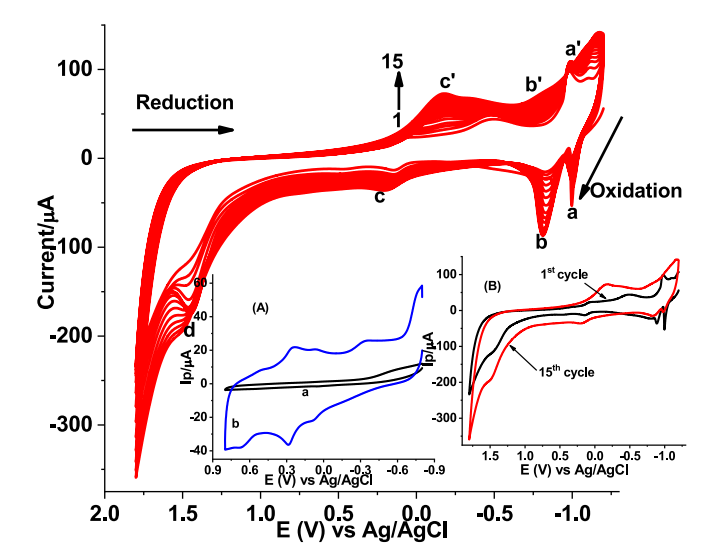


**Fig. 2.** CVs of GCE in pH 7.0 PBS containing 1.0 mM poly(C2)/GCE scanned in the range of -1.2 V to +1.8 V for 15 cycles at scan rate of 100 mV s $^{-1}$ . Inset: CVs of (A) (a) bare GCE, and (b) stabilized poly(C2)/GCE both scanned between the range of -0.8 - +0.8 V at 100 mV s $^{-1}$  in 0.5 M H<sub>2</sub>SO<sub>4</sub> and (B) 1st cycle and 15th cycle of polymerization.

in the Inset (B) shows that the anodic peak and cathodic peak current increased with scan cycles, indicating the polymer film deposition on the surface of the electrode. In addition to the one broad reductive peak at bare GCE in 0.5 M  $\rm H_2SO_4$ , the existence of several oxidative and reductive peaks at poly(C2)/GCE (curve an of inset (A)) indicated the creation of an electroactive polymer layer on the electrode surface.

#### 3.3. Characterization of poly(C2)/GCE electrochemically

#### 3.3.1. Cyclic voltammetric characterization

Further confirmation of the formation of coordination complexes between the metal and ligands was obtained through cyclic voltammetry and electrochemical impedance spectroscopy experiments. Figure SM4 demonstrates that the compounds polymerized on the GCE exhibit different electro-polymerization behaviors, indicating their distinct nature. Moreover, the voltammograms for C2 (Fig. SM4F) display additional distinct oxidative peaks compared to the intermediate complex (Fig. SM3D). This observation suggests the conversion of phen ligands to the C1 complex and the subsequent coordination of the precursor complex with 4,4'-bipy to form polymers of C3 and C2 complexes.

Ferricyanide, a redox-active species, plays a crucial role as an electrode transfer mediator and a potential standard. It is utilized for determining electrode areas and identifying issues related to new electrochemical cell designs. The plots in Fig. SM5 depict the anodic peak current (Ipa) as a function of the square root of the scan rate. The modified GCE, through a reduction in peak separation and a rise in peak current, exhibits electrocatalytic activity towards  $(Fe(CN)_6)^{3-/4}$ , indicating the successful deposition of a redox-active polymer film on the electrode surface [21,22,24].

Figure SM6 illustrates the cyclic voltammetric response of Fe(CN) $_6^{3-/4}$  on various forms of GCE. Compared to the naked GCE (a), the other modified GCEs display a pair of peaks with reduced peak-peak potential separation and improved current intensity. Generally, the electrodes for the probe's peak-peak separation go as follows: bare GCE ( $\Delta$ E 403) > poly(phen) ( $\Delta$ E 211) > poly(4,4′-bipy) ( $\Delta$ E 111) > poly(Co(0)) ( $\Delta$ E 95.3) > poly(C1) ( $\Delta$ E 102.8) > poly(C3) ( $\Delta$ E 90.6) > poly(C2) ( $\Delta$ E 83.8) (Fig. SM6). While the conductivity of the surface material mostly affects the peak-peak separation, the peak current intensity can be related to the electrode's resulting effective surface area [21,22]. The effective surface areas of the working electrodes were estimated using the slope value of the plot of Ipa versus  $\nu^{1/2}$  for (Fe(CN) $_6$ ) $^{3-/4-}$ , based on the Randles–Sevcik equation (Eq. (3)) [6,24].

$$I_{pa} = 2.69 \times 10^5 n^{3/2} A D^{1/2} \nu^{1/2} C_o$$
 (3)

Where n is the number of electron transfers, A is the electrode's active surface area, D is the diffusion coefficient, Co is the bulk concentration of  $\text{Fe}(\text{CN})_6^{3-/4}$ , v is the scan rate, and Ipa stands for the anodic peak current.

The computed functional surface areas of the investigated working electrodes are displayed in Table SM3. The enhanced current may therefore be caused by the much larger functional surface area of the poly(C2)/GCE for the probe, which is more than five times larger than that of the unmodified GCE.

# 3.3.2. Characterization using electrochemical impedance spectroscopy

The conductivity of synthesized coordination polymers was studied in order to investigate their electrical properties which interface between the surface of modified electrode and electrolyte [6]. EIS was employed to characterize the bare GCE, ligands, and intermediate and new coordination polymers of complexes. To investigate the ligands, intermediate and new coordination polymers of complexes, and the bare GCE, EIS was used. It is clear from the results that the first new synthesized coordination polymer of C2 complex has a high conductivity as compared from the precursor and the new coordination polymer complexes (Fig. 3). A high conductivity of C2 (Fig. 3g), makes it a good

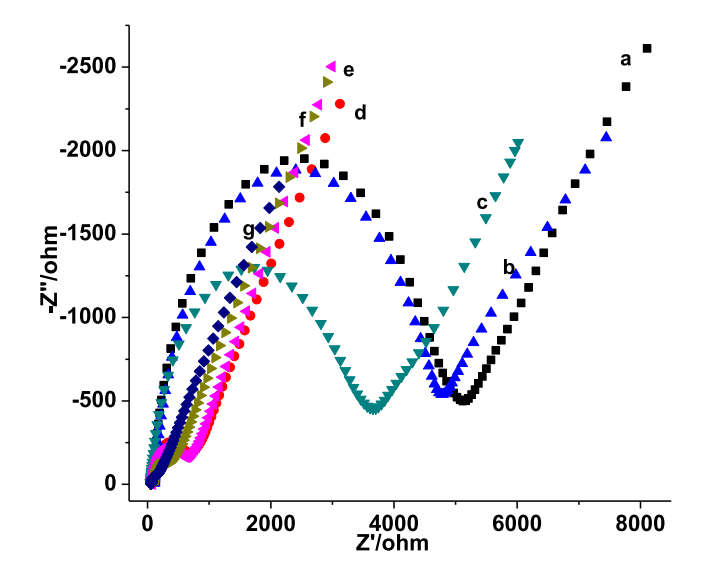


**Fig. 3.** Nyquist plots of (a) bare GCE, (b) poly(phen)/GCE, (c) poly(4,4'-bipy)/GCE, (d) poly(Co(0))/GCE, (e) poly(C1)/GCE, (f) poly(C3)/GCE, and (g) poly (C2)/GCE in pH 7.0 PBS containing 10.0 mM Fe(CN) $_6^{3-/4-}$  in 0.1 M KCl. Frequency range: 0.01–100,000 Hz, amplitude: 0.01 V, and potential: 0.23 V.

conducting material and potentially useful for sensor applications.

The figure clearly demonstrates a significant reduction in the diameter of the semi-circle region in the coordination oligomer of poly(C2)/ GCE compared to the bare GCE, poly(phen)/GCE, poly(4,4-bipy)/GCE, poly(C1)/GCE, and the final coordination polymer of poly(C3)/GCE. The unexpected superior performance of poly(C2)/GCE compared to poly(C3)/GCE can be explained by the fact that although C3 is five times larger in size, during the electropolymerization process, it may lead to the formation of a surface with smaller pores compared to C2. This reduced porosity in poly(C3)/GCE results in higher resistance, consequently diminishing its overall performance in comparison to poly(C2)/ GCE. The observed improvement in surface conductivity suggests a significant enhancement in the electron transfer channel among the analyte and the electrode substrate. This, in turn, expedites the migration of electroactive species from the bulk into the solution. The conductivity of coordination polymers tends to increase with larger pore sizes, indicating that compounds with larger pores exhibit higher conductivity compared to intermediate and final polymer complexes. This observation confirms the formation of coordination between the ligand and the new coordination polymer complex. Because more space permits electron conduction across porous structures, it follows that the conductivity of coordination polymers is directly correlated with the pore size.

The circuit elements for each electrode under study are summarized in Table 1, including double layer capacitance (Cdl), charge transfer resistance (Rct), and solution resistance (Rs), which are determined from the corresponding Nyquist plot using Eq. (4).

$$C_{dI} = \frac{1}{2\pi R_{cf}f} \tag{4}$$

Where  $C_{dI}$  – double layer capacitance, f – frequency corresponding to the imaginary resistance at its highest value and,  $R_{ct}$  – charge transfer resistance.

Eqs. (5) and (6) were utilized for calculating the surface roughness  $(R_F)$  of poly(C2)/GCE and the apparent heterogeneous electron transfer rate constant  $(k^0)$  value, respectively [22].

$$R_{\rm F} = \frac{C_{\rm dI}}{C_{\rm S}} \tag{5}$$

 Table 1

 Summary of calculated circuit elements for the studied for electrodes.

Electrode	$Rs/\Omega$ $cm^2$	<sup>a</sup> Rct/Ω cm <sup>2</sup>	<sup>b</sup> f /Hz	Cdl/ F	k <sup>0</sup>
GCE (curve a)	41.6	$5427 \pm 0.045$	$\begin{array}{c} 316.2 \pm \\ 0.031 \end{array}$	$\begin{array}{c} 9.3\times\\10^{-8}\end{array}$	$9.1 \times 10^{-8}$
poly(phen) (curve b)	41.6	$4840 \pm 0.041$	$93.3 \pm 0.026$	$3.5 \times 10^{-7}$	$3.43 \times 10^{-7}$
poly(4,4'-bipy) (curve c)	41.6	$3743 \pm 0.036$	$125.9 \pm \\ 0.024$	$\begin{array}{c} 3.4 \times \\ 10^{-7} \end{array}$	$6.13 \times 10^{-8}$
poly(Co(II)) (curve d)	41.6	$676 \pm 0.027$	$63.1 \pm \\ 0.021$	$\begin{array}{c} 3.7 \times \\ 10^{-6} \end{array}$	$2.75 \times 10^{-7}$
poly(C1) (curve e)	41.6	$\begin{array}{c} 606 \pm \\ 0.019 \end{array}$	$50.1 \pm \\ 0.017$	$\begin{array}{c} 5.2 \times \\ 10^{-6} \end{array}$	$2.6 \times 10^{-7}$
poly(C3) (curve f)	41.6	$\begin{array}{c} 286 \pm \\ 0.023 \end{array}$	$38.9 \pm 0.020$	$1.4\times\\10^{-5}$	$5.4 \times 10^{-7}$
poly(C2) (curve g)	41.6	$\begin{array}{c} 108 \pm \\ 0.016 \end{array}$	$17.8 \pm \\ 0.023$	$\begin{array}{c} 8.3 \times \\ 10^{-5} \end{array}$	$\begin{array}{c} 1.3\times\\10^{-6}\end{array}$

<sup>&</sup>lt;sup>a</sup> Mean Rct  $\pm$  RSD.

$$k^0 = \frac{RT}{F^2 A C R_{ct}} \tag{6}$$

Where R- the molar gas constant, T- temperature (298 K), F- Faraday constant (96,485C  $\mbox{mol}^{-1}$ ), C- the concentration of [Fe (CN)6]  $^{3-/4-}$ ; A- surface area of the electrode,  $C_{dI}$ , and  $C_S$  –the electrochemical double-layer capacitance of a planar and smooth electrode surface of the same material tested in the identical circumstances, respectively.

The obtained values for the heterogeneous electron transfer rate constant  $(k^0)$  of poly(C2)/GCE are 14.3 times higher than those of the unmodified GCE (Table 1). The slopes of the bare and poly(C2)-modified GCE surfaces are provided in Fig. SM5A and G, respectively. The roughness factor of poly(C2)/GCE is 3.5, clearly indicating an enhanced electrochemical activity for the redox probe on the novel  $[Co_{21}(phen)_{42}(bipy)_{21}]Cl_{42}$ -modified electrode surface.

# 3.4. Cyclic voltammetric investigation of CPF at poly(C2)/GCE

# 3.4.1. Electrochemical behavior of CPF

The obtained EIS results confirmed the new synthesized poly(C2)/GCE has been showed catalytic activity. The electrochemical behavior of CPF at unmodified GCE and six modified GCEs was studied using CV (Fig. 4). CPF exhibited an irreversible oxidation reaction on both the bare and modified electrodes. However, the potential was significantly reduced, and the current was enhanced by six-fold at the poly(C2)/GCE (curve b of inset), confirming the catalytic effect of the poly(C2)/GCE film in the oxidation of CPF. Furthermore, the observed potential and current benefits of CPF at poly(C2)/GCE compared to poly(phen)/GCE, poly(4,4'-bipy)/GCE, Co(0)/GCE, poly(C1)/GCE, and poly(C3)/GCE further support the suitability of poly(C2)/GCE for the quantification of CPF.

# 3.4.2. Scan rate impact on Epa and Ipa of CPF

Voltammograms for 0.5 mM CPF at pH 7.0 PBS at poly(C2)/GCE are shown in Fig. SM7 at a scan rate range of 10–200 mV s $^{-1}$ . It was confirmed that the oxidation of CPF at poly(C2)/GCE is irreversible by the peak potential shift of CPF observed with increasing scan rate.

From the result with lower correlation (R<sup>2</sup> value) between Ipa and scan rate than square root of scan rate (Fig. SM 7B & C), indicated that the oxidation kinetics of CPF at the poly(C2)/GCE was primarily governed by diffusion-controlled reaction [22,23]. This was also confirmed by the slope of 0.61 for the plot of log peak current versus log scan rate (Fig. SM7D), which is exactly in agreement with the ideal value [23]. Using the CV data, the number of electrons transported during the oxidation of CPF at the poly(C2)/GCE was calculated. Regarding the

 $<sup>^{\</sup>rm b}$  Mean f  $\pm$  RSD

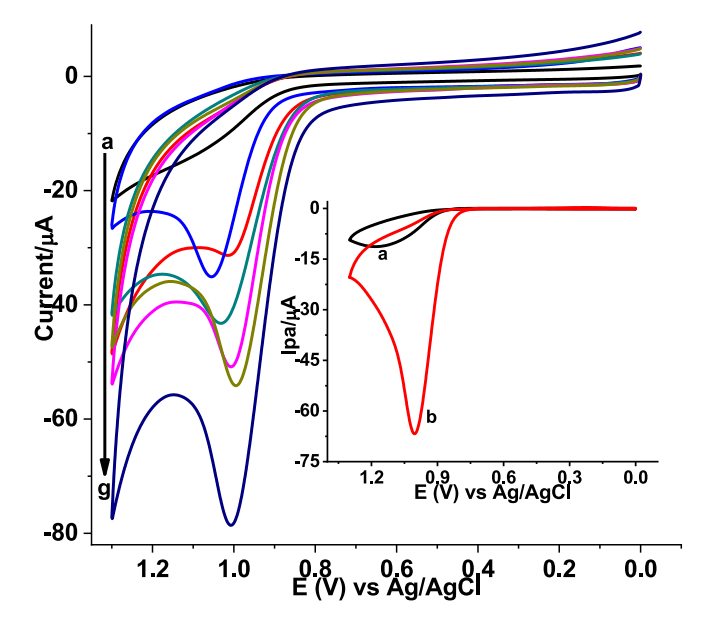


**Fig. 4.** CVs of bare GCE, poly(phen)/GCE, poly(4,4'-bipy)/GCE, poly(Co(0))/GCE, poly(C1)/GCE, poly(C3)/GCE, and poly(C2)/GCE (a-g, respectively) with the presence of 0.5 mM CPF in pH 7.0 PBS at scan rate 100 mV s $^{-1}$ . Inset: corrected for blank CVs of (a) bare GCE, and (b) poly(C2)/GCE.

instance of an irreversible process, the value of  $\alpha n$  was obtained by calculating the variation between the peak potential (Ep) and the half-wave potential (Ep1/2) using Eq. (7) [6].

$$E_{p} - E_{p1/2} = \frac{47.7}{qn} \tag{7}$$

Where  $\boldsymbol{\alpha}$  is the charge transfer coefficient and  $\boldsymbol{n}$  the number of electrons transferred.

Using Ep and Ep<sub>1/2</sub> values from the CV data at scan rate of 100 mV s<sup>-1</sup>, which are 1001 and 947 mV respectively, the value of  $\alpha n$  was computed to be 0.88. Assuming that  $\alpha$  for fully irreversible electrode process is 0.50 [31], an estimate of 1.76 (~2.0) electrons were transported during the oxidation of CPF at the poly(C2)/GCE surface, which is in agreement with other findings [26]. The relationship between *Ep* and  $\ln \nu$  for an irreversible process obeys the Eq. (8) [6].

$$Ep = E^{\circ} + \frac{RT}{(1-\alpha)nF} \left\{ 0.780 + ln \left( \frac{D_R^{\frac{1}{2}}}{k^{\circ}} \right) + ln \left[ \frac{(1-\alpha)nF\nu}{RT} \right]^{\frac{1}{2}} \right\}$$
(8)

Where  $E_P$  is the peak potential,  $E^0$  is the formal potential,  $\alpha$  is the electron transfer coefficient,  $k^0$  (s<sup>-1</sup>) is the electrochemical rate constant, and the other parameters have their usual meanings.

From the slope value of 0.031 for the fitted line (Epa (V) = 0.89 + 0.031 $ln\nu$ ) of the curve of plot of Ep versus ln(scan rate) (Fig. SM7), the value of n(1– $\alpha$ ) at the experimental temperature of 25 °C calculated using Eq. (8) was 0.94. Taking the two electrons for oxidation of CPF calculated using Eq. (7), the electron transfer coefficient ( $\alpha$ ) was calculated to be 0.53 confirming the irreversibility of the oxidation of CPF [6,24].

# 3.4.3. pH effect on Ipa and Epa of CPF

We can determine if a proton has taken part in the reaction, compute the proton: electron ratio, and explain the kind of interplay across the analyte and the electrode surface by looking at how pH affects the peak current and peak potential of an electroactive species at an electrode surface. Proton participation during the oxidation of CPF at the poly (C2)/GCE was indicated by an observed peak potential shift in the negative direction with pH variation from 4.5 to 8.5 (Fig. 5A). The slope of 0.055 for the plot of oxidative peak potential versus pH of the PBS (curve a in Fig. 5B) indicated a one: one ratio of protons and electrons involvement during the reaction process [23], which is very close to the ideal Nernst value (0.059 V/pH). A one:one ratio of protons and electrons involved during the reaction process was suggested by the slope of 0.055 (this is quite close to the optimum Nernst value (0.059 V/pH)), for the plot of the oxidative peak potential versus pH of the PB (curve an in Fig. 5B) [21].

As shown in the Fig, 5A, the oxidative peak current of CPF at the surface of poly(C2)/GCE increases from pH 4.5 to 7.0, and then decreases at pH values beyond it (curve b in Fig. 5B), making pH 7.0 the optimum. The increasing trend in current could be partially attributed to the coulomb forces of interaction between the CPF (pka: 6.1, and 8.6) [14], and the electrode modifier (poly(C2)) film (pka = 4.86 & 3.17, 4.82, phen, and 4,4'-bipy, respectively) [21,22,39]. Hence the observed increasing trend of current with pH from 4.5 - 7.0 may be accounted for the possible attraction between the cationic CPF (pka 6.1) and negatively charged modifier film.

Based on the calculated kinetic parameters using Eqs. ((7) and (8)) and the slope of Ipa versus pH, a reaction mechanism for the oxidation of CPF at poly(C2)/GCE was proposed (scheme SM3) which concurs with the mechanism in previously reported works [26].

# 3.5. DPV investigation of CPF at poly(C2)/GCE

Differential pulse voltammetry has proven to be highly valuable for

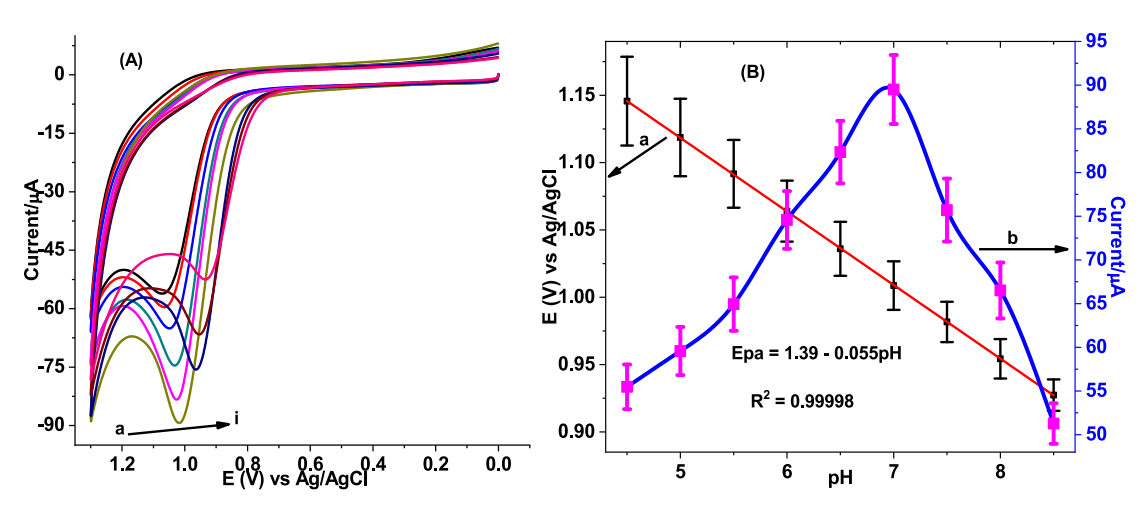


Fig. 5. (A) CVs of poly(C2)/GCE in PB of different pHs (a – i: 4.5, 5.0, 5.5, 6.0, 6.5, 7.0, 7.5, 8.0, and 8.5, respectively) containing 0.5 mM CPF, (B) plot of (a) Ep and (b) Ip vs. pHs in the entire pH range.

the sensitive detection of electro active compounds in pharmaceuticals, tissues, and biological samples [6,21,40]. DPV offers enhanced discrimination between Faradaic current and non-Faradaic current compared to cyclic voltammetry [21,40].

Figure SM8 illustrates the DPV curves of CPF obtained at both the unmodified GCE and the poly(C2)/GCE. As opposed to the oxidative peak observed in the bare electrode curve (a) inset, the poly(C2)/GCE (curve b of inset in Fig. SM8) exhibits a distinct, well-defined anodic peak with approximately six times higher current at a significantly reduced potential. This finding confirms the electrocatalytic role of the poly(C2)/GCE film in facilitating the oxidation of CPF.

To conduct a more detailed analysis, specific parameters of differential pulse voltammetry, namely the step potential and pulse amplitude, were optimized. Figure SM9 depicts the DPVs obtained at various step potentials (A) and amplitudes (B). The optimization process involved finding a balance between increasing the peak current and minimizing peak broadening. Consequently, the step potential of 6 mV and the pulse amplitude of 75 mV were determined as the optimal values.

# 3.6. Calibration curve

Using the optimized parameters and solution conditions, a calibration curve for CPF was constructed within the range of concentration for  $5.0 \times 10^{-8}\,\mathrm{M}$  to  $2.0 \times 10^{-4}\,\mathrm{M}$ . The detection limit (LoD) was determined as  $3.4 \times 10^{-9}\,\mathrm{M}$  (signal-to-noise ratio = 3, with n=7), and the limit of quantification (LoQ) was found to be  $1.14 \times 10^{-8}\,\mathrm{M}$  (Inset of Fig. 6). The method's low relative standard deviation (RSD) values, below 4.70 % for measurements made in triplicate, proved its accuracy and precision. This validation confirms the suitability and reliability of the proposed approach, which utilizes the newly synthesized mixed ligand Co(II) complex as an electrode modifier, for the detection of CPF in human urine samples and tablet formulations.

#### 3.7. DPV determination of CPF in real samples

# 3.7.1. Tablet sample

To evaluate the reliability of the  $poly([Co_{21}(phen)_{42}(bipy)_{21}]Cl_{42})/GCE$  sensor for CPF detection, differential pulse voltammograms were

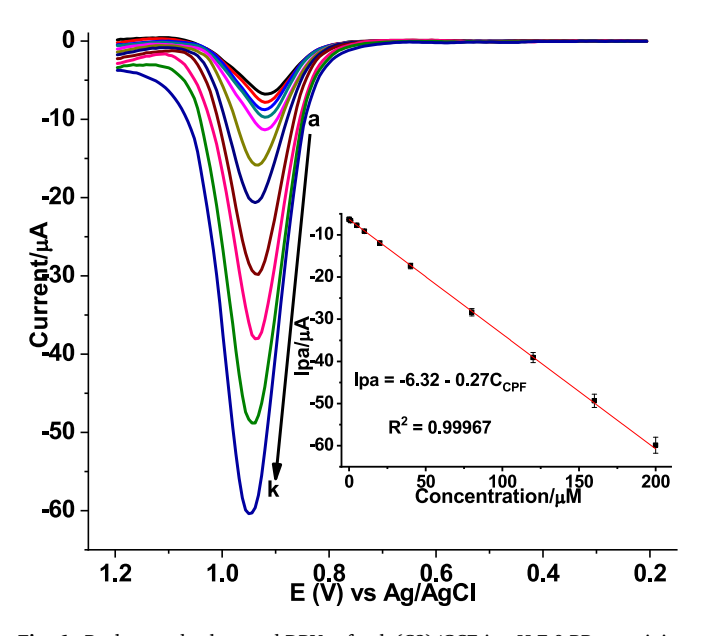


**Fig. 6.** Background subtracted DPVs of poly(C2)/GCE in pH 7.0 PB containing different concentrations of CPF (a-k: 0.05, 0.1, 1.0, 5.0, 10.0, 20.0, 40.0, 80.0, 120.0, 160.0, and 200.0  $\mu$ M, respectively). Inset: plot of Ipa vs. concentration of standard CPF.

recorded for 20.0  $\mu$ M nominal CPF concentrations of different tablet brands (Bruce, Aarciflox, Ciplet, and Zindolin) (Fig. SM10). The CPF content in each tablet brand was determined by applying the calibration regression equation (Inset of Fig. 6). The DPV oxidation peak current values for the detected CPF content of the four tablet brands were found to be 100.00 % (Bruce), 98.35 % (Ciplet), 101.30 % (Aarciflox), and 99.05 % (Zindolin) (Table 2). These findings verify that the developed method using the poly([Co<sub>21</sub>(phen)<sub>42</sub>(bipy)<sub>21</sub>]Cl<sub>42</sub>)/GCE as an electrode modifier is applicable for electrochemical sensor applications, demonstrating the suitability of the newly synthesized coordination polymer complex as a modifier.

#### 3.7.2. Human urine sample

Figure SM11 displays blank adjusted DPVs for human urine made according to the experimental section's procedure. The formation of a peak at a potential away from the characteristic potential for CPF (Fig. SM11 peak A & B), which is consistent with the documented literature [22], indicates the existence of electroactive species in the urine sample under analysis (peak A = uric acid, and peak B assign as creatinine for Fig. SM11) [22]. The analyzed human urine sample does not contain CPF, as indicated by the lack of a peak at the typical potential for CPF.

#### 3.8. Validation of the developed method

# 3.8.1. Recovery study

3.8.1.1. Human urine sample. Urine sample spiked was performed by adding 20.0, 40.0, 60.0, and 80.0  $\mu M$  CPF standard solutions to the urine sample that was evaluated under 3.7.2 (Fig. SM11). The urine sample showed peaks with the same current strength that were centered at around 254 mV and 617 mV (peak A & B), but without any spiking CPF levels, showing that the peak is not for CPF. The emergence of a third peak at the typical potential of CPF, whose current intensity improved with the amount of CPF spiked in the urine samples (curves b - e), however, suggests the peak in the unspiked urine is not CPF. The CPF spike recovery percentage in human urine samples ranges from 99.25 % to 100.51 % (Table SM4), with a percentage RSD value of less than 3.2 %, showed selectivity and accuracy of the method for determination of CPF in urine sample.

*3.8.1.2. Tablet samples.* To assess the spiking recovery of CPF in tablet samples, Ciplet brand tablet formulation samples was spiked with various concentrations of standard CPF (0.0, 20.0, 40.0, and 80.0) (Fig. SM12). The recovery results for the Ciplet tablet brand, as presented in Table 3, ranged from 99.44 % to 99.95 % with a %RSD value below 2.7 %. These findings confirm the precision of the method for CPF determination in tablet formulations.

# 3.8.2. Interference study

Investigating the proposed sensor's selectivity towards potential interfering compounds is crucial for determining the CPF in actual

**Table 2**A brief overview of the identified CPF content and the percentage of detected content compared to the nominal value for every tablet brand under analysis.

Tablet brand	Labeled CPF (mg/tablet)	Nominal CPF in sample (μM)	Detected CPF sample (μM) <sup>a</sup>	Detected CPF (%) <sup>b</sup>
Bruce	500	20.0	$20.00\pm0.025$	$100.00 \pm \\2.5$
Ciplet	500	20.0	$19.67\pm0.021$	$98.35 \pm 2.1$
Aarciflox	500	20.0	$20.26\pm0.023$	$101.30 \pm \\2.3$
Zindolin	500	20.0	$19.81\pm0.024$	$99.05 \pm 2.4$

 $<sup>^{\</sup>rm a}$  Detected mean CPF  $\pm$  RSD.

 $<sup>^{\</sup>rm b}$  Detected mean % CPF  $\pm$  %RSD.

**Table 3**Summary of recovery results of spikes of standard CPF in Ciplet brand tablet samples.

Tablet brand	Initial CPF content/ (μM)	Spiked CPF (μM)	Detected CPF (µM) <sup>a</sup>	Recovery (%) <sup>b</sup>
Ciplet	19.67	_	$19.67\pm0.025$	_
	19.67	20.00	$39.56 \pm 0.027$	$99.44 \pm 2.7$
	19.67	40.00	$59.60\pm0.017$	$99.64 \pm 1.7$
	19.67	80.00	$99.63\pm0.023$	$99.95 \pm 2.3$

 $<sup>^{\</sup>rm a}$  Detected mean CPF  $\pm$  RSD.

samples and assessing the sensor's commercial value. Drugs that might be found in CPF tablets or that share structural similarities with CPF and are frequently administered with CPF were chosen for the interference investigations.

3.8.2.1. Tablet sample. The impacts of selected potential interferents (ampicillin (AMP), cloxacillin (CLOX), chloroquine phosphate (CQP), and norfloxacin (NFN)) were investigated at various concentrations (Fig. SM13(A - D)). Interestingly, the tablet samples noticed CPF level showed an associated error of less than 4.73% even with interfering substance present (Table SM6). It indicates that the existence of interfering chemicals has no effect on the poly(C2)/GCE sensor's ability to detect CPF in the tablet sample. The finding holds great significance for the proposed sensor's commercial feasibility.

# 3.8.3. Reproducibility and stability studies

Assessing the reproducibility and stability of a sensor is crucial for ensuring its quality. Within this investigation, the developed sensor (poly(C2)/GCE) was subjected to reproducibility testing by measuring the current responses in seven consecutive DPV measurements taken over a span of seven weeks. Remarkably, the error observed in these measurements was only 3.15 % (%RSD) (Fig. SM14), indicating the high reproducibility and stability of the developed sensor.

# $3.9.\,$ Evaluation of the current approach in relation to previously published methods

The study assessed how well the novel approach performed in comparison to earlier research findings on the linear dynamic range, detection limit, and substrate type used for modification.

Compared to other reported approaches, the current method which uses a created unique mixed ligand complex modified electrode (poly (C2)/GCE)/GCE) offers the lowest LoD and the widest linear dynamic range (Table 4). As a result, the current approach, which makes use of the new modifier, may be a great choice for determining CPE in a variety of real samples.

# 4. Conclusions

The analysis confirmed the successful synthesis of the targeted oligomeric monomer complexes. Results from electrochemical impedance spectroscopy and cyclic voltammetric assessments validated the formation of an electroactive poly(C2) film on the surface of the glassy carbon electrode (GCE), enhancing both conductivity and surface area. The poly(C2)/GCE combination exhibited remarkable electrocatalytic capabilities for the oxidation of CPE. Utilizing a differential pulse voltammetric technique based on the poly(C2)/GCE setup, CPE levels were determined in tablet formulations from four different brands as well as in human urine samples characterized by complex matrices. The method demonstrated exceptional spike recovery rates, minimal interference, a broad linear dynamic range, a notably low detection threshold, and exceptional reproducibility and stability, showcasing its utility in quantifying CPE across diverse real samples. Notably, the sensor's

**Table 4**The created method's performance compared to a selected reported works.

Substrate	Modifier	Method	Dynamic range (µM)	LoD (µM)	Ref.
CPE	CZF-CME	AdSDPV	9.09-4700	0.0028	[26]
GCE	graphene	AdSWV	0.5-200	0.02	[41]
GCE	MIP	DPV	50-5000	12	[8]
SPE	rGO	AdSDPV	1.0-8.0	0.3	[35]
GCE	(Ca <sub>10</sub> (PO <sub>4</sub> ) <sub>6</sub> (OH) <sub>2</sub> ) sub-MPs	SWV	0.01-1310.0	0.0918	[3]
GCE	f-MWCNT@Poly- Aniline	LSV	0.1–1.0 1.0–20.0	0.08	[20]
SPE	mag@MIP-CB-NF	DPV	0.5-7.0	0.0084	[40]
GCE	Poly(C2)	DPV	0.05–200.0	0.0034	This work

efficacy was confirmed through the analysis of CPE content in various tablet samples, yielding values ranging from 98.35 % to 101.30 % of their expected concentrations. This newly devised approach proved particularly adept at assessing CPE in samples with intricate matrices, such as pharmaceutical products and human urine, outperforming previously described sensor methodologies.

# **Funding**

This research did not receive any specific grant from funding agencies in the public, commercial, or not-for-profit sectors.

#### CRediT authorship contribution statement

Mezgebu Biresaw: Writing – review & editing, Writing – original draft, Validation, Supervision, Software, Resources, Methodology, Investigation, Formal analysis, Data curation, Conceptualization. Adane Kassa: Writing – review & editing, Writing – original draft, Validation, Supervision, Software, Resources, Methodology, Investigation, Formal analysis, Data curation, Conceptualization. Getinet Tamiru Tigineh: Writing – review & editing, Writing – original draft, Validation, Software, Resources, Methodology, Investigation, Formal analysis, Data curation, Conceptualization. Atakilt Abebe: Writing – review & editing, Writing – original draft, Validation, Supervision, Software, Resources, Methodology, Investigation, Formal analysis, Data curation, Conceptualization.

# Declaration of competing interest

There is no any conflicting interest among the authors.

#### Data availability

The data supporting this article have been included as part of the Supplementary Information.

### Acknowledgements

The authors thank the Addis Pharmaceutical Factory (APF), Debre Markos University, Bahir Dar University's College of Science, the Ethiopian Food and Drug Administration Authority (EFDA), for providing us with standards and laboratory resources, respectively. The International Science Program (ISP) is acknowledged by the authors for providing financial assistance for the purchase of solvents and chemicals.

# Appendix A. Supplementary data

Supplementary data to this article can be found online at https://doi. org/10.1016/j.sbsr.2024.100721.

 $<sup>^{\</sup>rm b}\,$  % Recovery CPF  $\pm$  %RSD.

#### References

- [1] A. Abebe, T. Hailemariam, Synthesis and assessment of antibacterial activities of ruthenium (III) mixed ligand complexes containing 1, 10-phenanthroline and guanide, Bioinorg, Chem. Appl. 2016 (2016).
- [2] A. Abebe, G. Tamiru, A hexacationic coordination compound from Co (II) and a cationic ligand derived from 4, 4'-bipyridine: synthesis, characterization and investigation for biological application, Cogent Chem. 4 (1) (2018) 1564162.
- [3] S. Anitta, C. Sekar, Voltammetric determination of paracetamol and ciprofloxacin in the presence of vitamin C using cuttlefish bone-derived hydroxyapatite submicroparticles as electrode material, Res. Chem. 5 (2023) 100816.
- [4] R. Arab Ahmadi, F. Hasanvand, G. Bruno, H. Amiri Rudbari, S. Amani, Synthesis, spectroscopy, and magnetic characterization of copper (II) and cobalt (II) complexes with 2-amino-5-bromopyridine as ligand, Int. Schol. Res. Notices 2013 (2013).
- [5] A. Atakilt, G. Bayissa, A. Sendek, M. Kibret, Cobalt (II) complexes with 1, 10-phenanthroline alone and mixed with cytoside: synthesis and antibacterial activities, Ethiop. J. Sci. Technol. 11 (2) (2018) 79–96.
- [6] A.J. Bard, L.R. Faulkner, Fundamentals and applications, Electrochem. Methods 2 (482) (2001) 580–632.
- [7] N. Bäumer, J. Matern, G. Fernández, Recent progress and future challenges in the supramolecular polymerization of metal-containing monomers, Chem. Sci. 12 (37) (2021) 12248–12265.
- [8] Gürler Akyüz Berrin, Sabriye Perçin Özkorucuklu, Esengül Kır, Gizem Yıldırım Baştemur, Determination of ciprofloxacin in pharmaceutical dosage, human serum and urine, using molecularly imprinted polymer modified electrode by voltammetry, Eur. J. Sci. Technol. 20 (2020) 859–865.
- [9] Z. Bitew, A. Kassa, B. Misgan, Poly (diphenylamine-4-sulfonic acid) modified glassy carbon electrode for voltammetric determination of gallic acid in honey and peanut samples, Arab. J. Chem. 15 (7) (2022) 103853, https://doi.org/10.1016/j. arabic.2022.103853.
- [10] R. Chauhan, A.A. Gill, Z. Nate, R. Karpoormath, Highly selective electrochemical detection of ciprofloxacin using reduced graphene oxide/poly (phenol red) modified glassy carbon electrode, J. Electroanal. Chem. 871 (2020 Aug 15) 114254.
- [11] J. Chuiprasert, S. Srinives, N. Boontanon, C. Polprasert, N. Ramungul, A. Karawek, S.K. Boontanon, Ciprofloxacin electrochemical sensor using copper-iron mixed metal oxides nanoparticles/reduced graphene oxide composite, ACS Omega (2024 May 21).
- [12] J. Coates, Interpretation of Infrared Spectra, a Practical Approach, 2000.
- [13] A. Debalke, A. Kassa, T. Asmellash, Y. Beyene, M. Amare, G.T. Tigineh, A. Abebe, Synthesis of a novel diaquabis (1, 10-phenanthroline) copper (II) chloride complex and its voltammetric application for detection of amoxicillin in pharmaceutical and biological samples, Heliyon 8 (10) (2022).
- [14] M.E. Draz, D. El Wasseef, N. El Enany, M.E. Wahba, Green approach for tracking the photofate of ciprofloxacin and levofloxacin in different matrices adopting synchronous fluorescence spectroscopy: a kinetic study, R. Soc. Open Sci. 10 (1) (2023) 221086.
- [15] M.H. El Demeiry, S. Emara, Y. Abuleila, A. Ali, G. Hadad, R. Abdel Salam, A review article on Ciprofloxacin determination with various analytical techniques, Rec. Pharm. Biomed. Sci. 5 (Chemistry) (2021) 28–32.
- [16] A.E. Ejele, L.N. Ukiwe, C.K. Enenebeaku, N.U. Ejele, Evaluation of drug quality (III): determination of ciprofloxacin hydrochloride concentration in pharmaceutical tablets, Niger. J. Chem. Res. 20 (2015) 19–28.
- [17] K. Elgendy, M. Zaky, T.A. Eldin, S. Fadel, Rapid HPLC determination of ciprofloxacin, ofloxacin, and marbofloxacin alone or in a mixture, Res. Chem. 5 (2023) 100749.
- [18] S.B.J.A. Furniss, Practical organic Chemistry, 1989. New York.
- [19] N. Gissawong, S. Srijaranai, S. Boonchiangma, P. Uppachai, K. Seehamart, S. Jantrasee, E. Moore, S. Mukdasai, An electrochemical sensor for voltammetric detection of ciprofloxacin using a glassy carbon electrode modified with activated carbon, gold nanoparticles and supramolecular solvent, Microchim. Acta 188 (6) (2021 Jun) 208.
- [20] P. Jain, R.V. Motghare, Electro-oxidation and determination of ciprofloxacin at f-MWCNT@ poly-aniline glassy carbon electrode, J. Electrochem. Soc. 169 (5) (2022) 05651.
- [21] A. Kassa, A. Abebe, M. Amare, Synthesis, characterization, and electropolymerization of a novel Cu (II) complex based on 1, 10-phenanthroline for electrochemical determination of amoxicillin in pharmaceutical tablet formulations, Electrochim. Acta 384 (2021) 138402, https://doi.org/10.1016/j. electracta 2021 138402
- [22] A. Kassa, A. Abebe, G. Tamiru, M. Amare, Synthesis of a Novel [diresorcinate-1, 10phenanthrolinecobalt (II)] Complex, and Potentiodynamic Fabrication of Poly

- (DHRPCo)/GCE for Selective Square Wave Voltammetric Determination of Procaine Penicillin G in Pharmaceutical and Biological Fluid Samples, ChemistrySelect 7 (1) (2022) e202103458, https://doi.org/10.1002/slct.202103458.
- [23] A. Kassa, M. Amare, Poly (4-amino-3-hydroxynaphthalene-1-sulfonic acid) modified glassy carbon electrode for square wave voltammetric determination of amoxicillin in four tablet brands, BMC Chem. 15 (2021) 1–11, https://doi.org/10.1186/s13065-021-00739-0.
- [24] A. Kassa, G.T. Tigineh, A. Abebe, Electrochemical determination of chloroquine phosphate in real samples using a diresorcinate-1, 10-phenanthrolinecobalt (II)modified glassy carbon electrode, ChemistryOpen 12 (3) (2023) e202300004.
- [25] M.A. Khaleque, M.R. Ali, M.A. Aly, M.I. Hossain, K.H. Tan, M.A. Zaed, R. Saidur, M. M. Rahman, N.M. Mubarak, M.Z. Khan, Highly sensitive electrochemical detection of ciprofloxacin using MXene (Ti3C2Tx)/poly (rutin) composite as an electrode material, Diam. Relat. Mater. (2024 Nov 5) 111749.
- [26] M.P. Kingsley, P.K. Kalambate, A.K. Srivastava, Simultaneous determination of ciprofloxacin and paracetamol by adsorptive stripping voltammetry using copper zinc ferrite nanoparticles modified carbon paste electrode, RSC Adv. 6 (18) (2016) 15101–15111.
- [27] I. Kośka, K. Purgat, R. Głowacki, P. Kubalczyk, Simultaneous determination of ciprofloxacin and ofloxacin in animal tissues with the use of capillary electrophoresis with transient pseudo-isotachophoresis, Molecules 26 (22) (2021) 6931.
- [28] I. Kośka, K. Purgat, P. Kubalczyk, Simple, fast and reliable CE method for simultaneous determination of ciprofloxacin and ofloxacin in human urine, Sci. Rep. 12 (1) (2022) 7729.
- [29] H. Kumagai, Y. Tamaki, O. Ishitani, Photocatalytic systems for CO2 reduction: metal-complex photocatalysts and their hybrids with photofunctional solid materials, Acc. Chem. Res. 55 (7) (2022) 978–990.
- [30] S. Kumaresan, P. Ramadevi, Molecular Ribbons: Hydrothermal Synthesis and Structural Characterization of [{Cu (dipic)(H2O)} 2 (μ-4, 4'-bipy)]. 2H2O (Dipic= Pyridine-2, 6-Dicarboxylato; 4, 4'bipy= 4, 4'-Bipyridyl), 2005.
- [31] E. Laviron, General expression of the linear potential sweep voltammogram in the case of diffusionless electrochemical systems, J. Electroanal. Chem. Interfacial Electrochem. 101 (1) (1979) 19–28.
- [32] T.Y. Mahmoud, I.S. Hamza, A.L. Jarallah, Spectrophotometric method for the determination of ciprofloxacin in pure and pharmaceutical preparations: development and validation, Eng. Proc. 59 (1) (2024) 164.
- [33] A. Mebrie, M. Amare, A. Kassa, Y.B. Yohannes, A. Tesfaye, A. Abebe, T. Asmelash, Novel poly (diaquabis (1, 10-phenanthroline) copper (II) chloride) modified glassy carbon electrode for square wave voltammetric determination of aspirin in tablet samples, Sens. Int. 3 (2022) 100187.
- [34] B. Meunier, G. Brudvig, J.L. Mclain, S.I. Murahashi, V.L. Pecoraro, D. Riley, A. Robert, J.A. Rodriguez, R.A. Sheldon, H. Zhu (Eds.), Biomimetic Oxidations Catalyzed by Transition Metal Complexes, World Scientific, 2000.
- [35] M. Pan, P. Guo, H. Liu, J. Lu, Q. Xie, Graphene oxide modified screen-printed electrode for highly sensitive and selective electrochemical detection of ciprofloxacin residues in milk, J. Anal. Sci. Technol. 12 (1) (2021) 1–7.
- [36] R. Scherer, J. Pereira, J. Firme, M. Lemos, M. Lemos, Determination of ciprofloxacin in pharmaceutical formulations using HPLC method with UV detection, Indian J. Pharm. Sci. 76 (6) (2014) 541.
- [37] J. Takaya, Catalysis using transition metal complexes featuring main group metal and metalloid compounds as supporting ligands, Chem. Sci. 12 (6) (2021) 1964–1981.
- [38] D.L. Tennent, D.R. McMillin, A detailed analysis of the charge-transfer bands of a blue copper protein. Studies of the nickel (II), manganese (II), and cobalt (II) derivatives of azurin, J. Am. Chem. Soc. 101 (9) (1979) 2307–2311.
- [39] O. Toma, N. Mercier, M. Allain, C. Botta, Protonated N-oxide-4, 4'-bipyridine: from luminescent Bi III complexes to hybrids based on H-bonded dimers or H-bonded open 2D square supramolecular networks, CrystEngComm 15 (42) (2013) 8565–8571.
- [40] A. Wong, M. Santos, T. Silva, F.C. Moraes, O. Fatibello-Filho, M.D. Sotomayor, Sensitive and selective voltammetric determination of ciprofloxacin using screenprinted electrodes modified with carbon black and magnetic-molecularly imprinted polymer, Electroanalysis 35 (1) (2023) e202200165, https://doi.org/ 10.1002/elan.202200165.
- [41] A.J. Xie, Y. Chen, S.P. Luo, Y.W. Tao, Y.S. Jin, W.W. Li, Electrochemical detection of ciprofloxacin based on graphene modified glassy carbon electrode, Mater. Technol. 30 (6) (2015) 362–367.
- [42] L. Zhu, R. Bakhtiar, N.M. Kostić, Transition-metal complexes as alternatives to proteolytic enzymes. Regioselective cleavage of myoglobin by palladium (II) aqua complexes, J. Biol. Inorg. Chem. 3 (1998) 383–391.